Article

Influence of Integration Schemes and Maneuvers on the Initial Alignment and Calibration of AUVs: Observability and Degree of Observability Analyses

Adriano Frutuoso [1,*]**, Felipe O. Silva** [2] **and Ettore A. de Barros** [1]

[1] Unmanned Vehicles Laboratory, Department of Mechatronics Engineering, University of Sao Paulo, Avenida Professor Mello Moraes, 2231, Sao Paulo 05508-030, Brazil; eabarros@usp.br
[2] Department of Automatics, Federal University of Lavras, Lavras 37200-900, Brazil; felipe.oliveira@ufla.br
[*] Correspondence: adriano.frutuoso@usp.br

Abstract: The use of autonomous underwater vehicles (AUV) has increased in a wide range of sectors, including the oil and gas industry, military, and marine research. The AUV capabilities to operate without a direct human operator and untethered to a support vessel are features that have aroused interest in the marine environment. The localization of AUV is significantly affected by the initial alignment and the calibration of the navigation sensors. In this sense, this paper proposes a thorough observability analysis applied to the latter problem. The observability analysis is carried out considering three types of sensor fusion integration and a set of maneuvers, and the results are validated through numerical simulations. As main contribution of this paper, it is shown how the addition of position errors in the observation vector can decouple some gyro and accelerometer biases from the latitude and altitude errors, particularly in the stationary observability analysis. The influence of oscillations in the diving plane and typical AUV maneuvers are analyzed, showing their relative impacts on the degree of observability of the inertial measurement unit (IMU)/Doppler velocity log (DVL) misalignment and DVL scale factor error. Finally, the state's estimation accuracy is also analyzed, showing the limitation of the degree of observability as an assessment tool for the estimability of the states.

Keywords: AUV; observability analysis; degree of observability

1. Introduction

Technological advances in recent years have promoted the development of autonomous vehicles for a wide variety of sectors, including aerial, aquatic, and terrestrial applications. Internet of Things and smart cities [1,2] inspection of oil and gas pipelines [3], swarm of underwater robots [4], and autonomous cars [5] are some examples of recent applications of autonomous vehicles.

Unlike terrestrial and aerial mobile robots, autonomous underwater vehicles (AUV) should deal with particular boundaries related to the limited transmission of electromagnetic signals underwater. Those limits consist of the absence of the localization measures provided by satellite-based systems, and the absence of a high band and long range communication with the human user who is at the surface. The first kind of limitation has an impact at AUV self-localization, which is the subject of this work.

The initial alignment, which consists of determining the initial orientation of the vehicle, and the calibration of the navigation sensors are key factors that significantly influence the performance of AUV navigation.

The inertial measurement unit (IMU), Doppler velocity log (DVL), pressure sensor (PS), and global positioning system (GPS) are navigation sensors widely used in AUVs [6]. Therefore, the proper estimation of the navigation sensor errors, e.g., inertial sensors biases,

DVL scale factor error, and the misalignment between the IMU and the DVL, as well as the alignment errors, are necessary to improve navigation performance.

The dynamic and observation models and the movements executed by the AUV affect the performance of the estimation. In this sense, the observability analysis is important to determine the efficiency of the Kalman filter in the estimation of the states [7].

A system is said to be observable if the initial states, at time t_0, can be determined at time t_1, from observations of the inputs and outputs of the system taken at $[t_0, t_1]$ [8]. The observability analysis can be classified as qualitative and quantitative [9]. The qualitative analysis is a binary criterion, defining only whether the system or its states are observable or unobservable. This criterion was first proposed by Kalman [10]. The quantitative analysis, in turn, defines how observable the system or its states are. This analysis is related to the concept of the degree of observability.

According to Friedman [9], the rank of the observability matrix, its linearly independent columns, eigenvalues, singular values, and determinant are some metrics used to analyze the observability of a system. In particular, the matrix rank is extensively employed in the qualitative analysis. Concerning the degree of observability, it can be calculated using the degree of independence between the columns (or the singular values) of the observability matrix/Grammian. The singular values, in particular, are largely employed to determine the degree of observability numerically [11–15].

In the last years, observability analysis has been employed to the AUV navigation problem, especially during its initial alignment and calibration phase, to evaluate the observability of the navigation variables subject to maneuver conditions [14,16–20]. In [16], it was shown that the observability of the DVL velocity error in the navigation frame is influenced by the AUV angular movement. However, the dynamic model used in the analysis did not include the vertical velocity error and the altitude error. Furthermore, the misalignment between the IMU and the DVL and the DVL scale factor error were not directly included in the dynamic model.

In [17], analytical expressions were derived for the UnObservable Subspace (UOS) of the AUV navigation problem, considering the following maneuvers: (1) stationary, (2) stationary with yaw angle variation, and (3) constant speed with yaw angle variation. The UOS derivation was performed based on the determination of the kernel of the observability Grammian. However, the IMU/DVL misalignment and the DVL scale factor error were, again, not included in the analysis. As a consequence, in the inertial navigation system (INS)/DVL integration for the AUV static condition, the dimension of the UOS was found to be 4, comprising the gyro bias error in the z-axis, the vertical alignment error, and linear combinations of the north and east alignment errors with the accelerometer bias errors in the x and y axes. Such a UOS dimension, however, is in disagreement with other works [21,22], for which the dimension of the UOS, in the stationary case, was 3 (obviously disregarding the position errors). For Bar-Itzhack and Berman [21], and Silva, Hemerly, and Leite Filho [22], such UOS comprises linear combinations of the accelerometer bias errors in the north and east directions with the alignment errors in the north and east, plus a linear combination of the vertical alignment error with the gyro bias error in the east direction.

In addition, the dynamic model of INS error propagation presented in [17] did not include the coupling term between the attitude error vector and the velocity error vector, which contributed to the attainment of a UOS dimension equal to 4. In this sense, the dynamic model of [17] can be seen as a simplification of the dynamic model presented in [23], particularly chosen to facilitate the computation of the kernel of the observability Grammian.

In [18], it was demonstrated that trajectories containing segments of type I (constant attitude with linearly independent specific force variation in the body frame) and type II (turning segments) make the attitude errors, the velocity errors, the inertial sensors biases, the IMU/DVL misalignment, and the DVL scale factor error observable. However, the degrees of observability of the state variables were not evaluated. The results of [19] pointed out that the addition of vertical and translational movements in the AUV trajectory

make the variables associated with the DVL calibration completely observable. The results presented in [14,20] further show that the degrees of observability of the state variables increased with changes in the direction of the trajectory.

In [14,19,20], however, the authors did not address the couplings between the state variables, which are not distinguished by the Kalman filter [21]. Furthermore, in [19], the variables associated with the initial alignment and the biases of the inertial sensors were not included in the observability analysis. In [20], in turn, the IMU/DVL misalignment was disregarded from the analysis, while in [14], the degrees of observability of the DVL scale factor errors and the IMU/DVL misalignment were not evaluated.

Given the aforementioned open issues, this work performs quantitative and qualitative observability analyses regarding the problem of the initial alignment and the calibration of the navigation sensors of the AUV. The quantitative analysis is performed by the rank computation, and the qualitative analysis is performed by the degree of observability computation. The observability analysis is carried out considering three types of sensor fusion integration and a set of maneuvers: (1) stationary, (2) mooring, (3) straight-line with constant speed, (4) straight-line with acceleration, (5) zigzag, (6) lawn mower with constant speed, and (7) lawn mower with zigzag and swing. The observability analysis results are particularly useful in the AUV mission planning, in terms of the choice of the better maneuver and the definition of the appropriated integration.

Numerical simulations are carried out to generate the results. In the stationary observability analysis, it is shown how the addition of position errors in the observation vector can decouple some gyro and accelerometer biases from the latitude and altitude errors. The influence of oscillations in the diving plane and typical AUV maneuvers is also analyzed, showing their relative impacts on the degree of observability of the IMU/DVL misalignment and DVL scale factor error. In addition, the accuracy of the state estimation is also analyzed, showing the limitation of the degree of observability as an assessment tool for the estimability of the states.

This paper is organized as follows: Section 2 presents the dynamic model and the observation models for the INS/GPS/DVL/PS, INS/DVL/PS, and INS/DVL integrations. In Section 3, the observability decomposition is presented. Section 4 is dedicated to the observability analysis of the AUV linear time-varying system using the stripped observability matrix and the singular value decomposition for the rank computation. Section 5 is dedicated to the evaluation of the corresponding degree of observability. Sections 6 and 7, lastly, present simulation results and the discussions, respectively. Section 8 is dedicated to the conclusions.

2. System Modelling

The expanded INS errors resolved in the NED (north-east-down) frame is given by Equation (1) [24,25], where $\mathrm{x} = \begin{bmatrix} \phi^n & \delta v^n & \delta L & \delta \lambda & \delta h & \mathrm{b_g} & \mathrm{b_a} & \mathrm{e} & s_f \end{bmatrix}^T$ is the state vector; $\phi^n = \begin{bmatrix} \phi_N & \phi_E & \phi_D \end{bmatrix}^T$ corresponds to the attitude error vector; δv^n is the velocity error vector; δL, $\delta \lambda$, δh are the latitude, longitude e altitude errors, respectively; $\mathrm{b_g}$ and $\mathrm{b_a}$ are the gyro and accelerometer bias; $\mathrm{w_g}$ and $\mathrm{w_a}$ are the gyro and accelerometer noises, respectively; $\mathrm{e} = \begin{bmatrix} e_x & e_y & e_z \end{bmatrix}^T$ and s_f correspond to the IMU/DVL misalignment errors and scale factor error of the DVL, respectively; C_b^n is the attitude matrix from the body frame to the navigation frame; ω_{in}^n is the angular rate of the navigation frame with respect to the inertial frame resolved in the navigation frame; and f^n is the specific force resolved in the navigation frame.

The coefficients of the INS error model are given by Equations (2)–(13), where R_N and R_E are the meridian and transverse radii of curvature, respectively; g is the local gravity; and Ω is the turn rate of the Earth. R_0 is computed as $R_0 = \sqrt{R_N R_E}$.

$$\dot{x} = \begin{bmatrix} -[\omega_{in}^n\times] & A_1 & A_2 & 0_{3\times1} & A_3 & -C_b^n & 0_{3\times3} & 0_{3\times4} \\ [f^n\times] & ([v^n\times]A_1 - A_4) & [v^n\times]A_5 & 0_{3\times1} & ([v^n\times]A_3 + C_5) & 0_{3\times3} & C_b^n & 0_{3\times4} \\ 0_{1\times3} & B_1 & 0 & 0 & b_2 & 0_{1\times3} & 0_{1\times3} & 0_{1\times4} \\ 0_{1\times3} & C_1 & c_2 & 0 & c_3 & 0_{1\times3} & 0_{1\times3} & 0_{1\times4} \\ 0_{1\times3} & C_4 & 0 & 0 & 0 & 0_{1\times3} & 0_{1\times3} & 0_{1\times4} \\ 0_{3\times3} & 0_{3\times3} & 0_{3\times1} & 0_{3\times1} & 0_{3\times1} & 0_{3\times3} & 0_{3\times3} & 0_{3\times4} \\ 0_{3\times3} & 0_{3\times3} & 0_{3\times1} & 0_{3\times1} & 0_{3\times1} & 0_{3\times3} & 0_{3\times3} & 0_{3\times4} \\ 0_{4\times3} & 0_{4\times3} & 0_{4\times1} & 0_{4\times1} & 0_{4\times3} & 0_{4\times3} & 0_{4\times3} & 0_{4\times4} \end{bmatrix} x + \begin{bmatrix} -C_b^n & 0_{3\times3} \\ 0_{3\times3} & C_b^n \\ 0_{1\times3} & 0_{1\times3} \\ 0_{1\times3} & 0_{1\times3} \\ 0_{1\times3} & 0_{1\times3} \\ 0_{3\times3} & 0_{3\times3} \\ 0_{3\times3} & 0_{3\times3} \\ 0_{4\times3} & 0_{4\times3} \end{bmatrix} \begin{bmatrix} w_g \\ w_a \end{bmatrix} \tag{1}$$

$$A_1 = \begin{bmatrix} 0 & \frac{1}{R_E+h} & 0 \\ -\frac{1}{R_N+h} & 0 & 0 \\ 0 & -\frac{\tan(L)}{R_E+h} & 0 \end{bmatrix} \tag{2}$$

$$A_2 = \begin{bmatrix} -\Omega\sin(L) \\ 0 \\ -\Omega\cos(L) - \frac{v_E\sec^2(L)}{R_E+h} \end{bmatrix} \tag{3}$$

$$A_3 = \begin{bmatrix} -\frac{v_E}{(R_E+h)^2} \\ \frac{v_N}{(R_N+h)^2} \\ \frac{v_E\tan(L)}{(R_E+h)^2} \end{bmatrix} \tag{4}$$

$$A_4 = \begin{bmatrix} 0 & 2\Omega\sin(L) + \frac{v_E\tan(L)}{R_E+h} & -\frac{v_N}{R_N+h} \\ -2\Omega\sin(L) - \frac{v_E\tan(L)}{R_E+h} & 0 & -2\Omega\cos(L) - \frac{v_E}{R_E+h} \\ \frac{v_N}{R_N+h} & 2\Omega\cos(L) + \frac{v_E}{R_E+h} & 0 \end{bmatrix} \tag{5}$$

$$A_5 = \begin{bmatrix} -2\Omega\sin(L) \\ 0 \\ -2\Omega\cos(L) - \frac{v_E\sec^2(L)}{R_E+h} \end{bmatrix} \tag{6}$$

$$B_1 = \begin{bmatrix} \frac{1}{R_N+h} & 0 & 0 \end{bmatrix} \tag{7}$$

$$b_2 = -\frac{v_N}{(R_N+h)^2} \tag{8}$$

$$C_1 = \begin{bmatrix} 0 & \frac{\sec(L)}{R_E+h} & 0 \end{bmatrix} \tag{9}$$

$$c_2 = \frac{\sec(L)\tan(L)v_E}{R_E+h} \tag{10}$$

$$c_3 = -\frac{v_E\sec(L)}{(R_E+h)^2} \tag{11}$$

$$C_4 = \begin{bmatrix} 0 & 0 & -1 \end{bmatrix} \tag{12}$$

$$C_5 = \begin{bmatrix} 0 \\ 0 \\ -\frac{2g}{R_0+h} \end{bmatrix} \tag{13}$$

Considering the INS/GPS/DVL/PS loosely coupled integrated navigation, the observation model is as follows:

$$y = \begin{bmatrix} \delta v^n \\ \delta L \\ \delta \lambda \\ \delta h \end{bmatrix} = \begin{bmatrix} v^n - \widetilde{v}_d^n \\ L - \widetilde{L}_{gps} \\ \lambda - \widetilde{\lambda}_{gps} \\ h - \widetilde{h}_{ps} \end{bmatrix} \tag{14}$$

$$y = Hx + \nu = \begin{bmatrix} -[v^n \times] & I_{3\times3} & 0_{3\times3} & 0_{3\times3} & 0_{3\times3} & -C_b^n \left[v^b \times \right] & -v^n \\ 0_{3\times3} & 0_{3\times3} & I_{3\times3} & 0_{3\times3} & 0_{3\times3} & 0_{3\times3} & 0_{3\times1} \end{bmatrix} x + \nu \tag{15}$$

where $\widetilde{v}_d^n$ represents the DVL velocity vector resolved in the navigation frame; $\widetilde{L}_{gps}$ and $\widetilde{\lambda}_{gps}$ are the GPS latitude and longitude, respectively; $\widetilde{h}_{ps}$ is the altitude from the PS measurements; and ν is the measurement noise vector.

Considering the loosely coupled INS/DVL/PS integration, the vector and the observation model are as follows:

$$y = \begin{bmatrix} \delta v^n \\ \delta h \end{bmatrix} = \begin{bmatrix} v^n - \widetilde{v}_d^n \\ h - \widetilde{h}_{ps} \end{bmatrix} \tag{16}$$

$$\begin{aligned} y &= Hx + \nu \\ &= \begin{bmatrix} -[v^n \times] & I_{3\times3} & 0_{3\times3} & 0_{3\times3} & 0_{3\times3} & -C_b^n \left[v^b \times \right] & -v^n \\ 0_{1\times3} & 0_{1\times3} & [\,0\ \ 0\ \ 1\,] & 0_{1\times3} & 0_{1\times3} & 0_{1\times3} & 0 \end{bmatrix} x + \nu \end{aligned} \tag{17}$$

For the loosely coupled INS/DVL integration:

$$y = \delta v^n = v^n - \widetilde{v}_d^n \tag{18}$$

$$y = Hx + \nu = \begin{bmatrix} -[v^n \times] & I_{3\times3} & 0_{3\times3} & 0_{3\times3} & 0_{3\times3} & -C_b^n \left[v^b \times \right] & -v^n \end{bmatrix} x + \nu \tag{19}$$

3. Observability Decomposition

Consider the linear and time-invariant (LTI) model:

$$\begin{cases} \dot{x}(t) = Ax(t) + Bu(t) \\ y(t) = Hx(t) + Du(t) \end{cases} \tag{20}$$

If the system is unobservable, there is a similarity transformation, shown in Equation (21), which results in the decomposed form of Equation (22), where the subsystem (A_{11}, B_1, H_1, D) is observable [8]. A_{11} is a square matrix $r \times r$, where r is the dimension of the observable subspace.

$$\begin{cases} \overline{x} = Tx \\ \overline{A} = TAT^{-1} \\ \overline{B} = TB \\ \overline{H} = HT^{-1} \\ \overline{D} = D \end{cases} \tag{21}$$

$$\begin{cases} \dot{\overline{x}}(t) = \begin{bmatrix} A_{11} & 0 \\ A_{21} & A_{22} \end{bmatrix} \overline{x}(t) + \begin{bmatrix} B_1 \\ B_2 \end{bmatrix} u(t) \\ y(t) = \begin{bmatrix} H_1 & 0 \end{bmatrix} \overline{x}(t) + Du(t) \end{cases} \tag{22}$$

The new state vector $\overline{x}$ corresponds to combinations of the observable and unobservable states of the original system. The similarity transformation does not change the observability of the original system [8].

The similarity transformation matrix is given by Equation (23), where $\langle v_1, v_2, ..., v_r \rangle$ is a set of linearly independent vectors of $\Re^n$. $\langle v_{r+1}, v_{r+2}, ..., v_n \rangle$ is a base of the kernel of the observability matrix Q_o:

$$T = \begin{bmatrix} v_1 & v_2 & \ldots & v_r & v_{r+1} & \ldots & v_n \end{bmatrix}^{-1} \tag{23}$$

$$Q_o v_i = 0, i = r+1, \ldots, n \tag{24}$$

where

$$Q_o = \begin{bmatrix} H \\ HA \\ HA^2 \\ \vdots \\ HA^{n-1} \end{bmatrix} \tag{25}$$

4. Stripped Observability Matrix and Singular Value Decomposition

Consider the linear time-varying (LTV) model for the continuous and discrete cases:

$$\begin{cases} \dot{x}(t) = A(t)x(t) \\ y(t) = H(t)x(t) \end{cases} \tag{26}$$

$$\begin{cases} x_{k+1} = \Phi_k x_k \\ y_k = H_k x_k \end{cases} \tag{27}$$

The observability of an LTV system in the time interval t_o to t_f can be determined from the analysis of the rank of the observability Grammian matrix O. The observability Grammian matrices for the continuous and discrete cases are as follows [9]:

$$O\left(t_o, t_f\right) = \int_{t_o}^{t_f} \Phi(t, t_o)^T H(t)^T H(t) \Phi(t, t_o) dt \tag{28}$$

$$O\left(k_o, k_f\right) = \sum_{k=k_0}^{k_f} \Phi\left(k, k_f\right)^T H_k^T H_k \Phi\left(k, k_f\right) \tag{29}$$

Equations (28) and (29) show that for the determination of O, it is necessary to calculate the state transition matrices, which are $\Phi(t, t_o)$ and $\Phi\left(k, k_f\right)$. If O is a non-singular matrix, the LTV system is observable in the considered time interval.

In general, the calculation of O is performed numerically [7,9]. As an alternative to O, the observability of the LTV system can be evaluated by the rank of Q_{SOM} (stripped observability matrix), which is obtained by partitioning the LTV system into piece-wise constant systems (PWCS) [7].

Then, consider the PWCS models for the discrete case:

$$\begin{cases} x_{k+1} = \Phi_j x_k \\ y_j = H_j x_k \end{cases} \tag{30}$$

For each j time segment, matrices Φ_j and H_j are constant. Then, Q_{SOM} is computed using Equation (31), where $Q_{o,j}$, for $j = 1, 2, \ldots, l$, corresponds to the observability matrix for each j time segment.

$$Q_{SOM}(r) = \begin{bmatrix} Q_{o,1} \\ Q_{o,2} \\ \vdots \\ Q_{o,l} \end{bmatrix} \tag{31}$$

The rank of a matrix can be numerically determined by singular value decomposition into (SVD) or by decomposition into eigenvalues. The rank corresponds to the number of singular values or eigenvalues different from zero [9]. Unlike eigenvalues, singular values are always equal to or greater than zero.

The SVD of a matrix $A \in \Re^{m \times n}$ is [13,15]:

$$A = U\Sigma V^T \tag{32}$$

where $U = \begin{bmatrix} u_1 & u_2 & \ldots & u_m \end{bmatrix}$ and $V = \begin{bmatrix} v_1 & v_2 & \ldots & v_n \end{bmatrix}$ are the orthogonal matrices, $\Sigma = diag(S, 0)$, $\Sigma \in R^{m \times n}$, is a matrix of singular values, and $S = diag(\sigma_1, \sigma_2, \sigma_3, \ldots, \sigma_n)$, with $\sigma_1 \geq \sigma_2 \geq \sigma_3 \geq \ldots \geq \sigma_n$, which corresponds to a diagonal matrix containing the singular values of A.

Then, an LTV system is observable if Q_{SOM} is full rank. On the contrary, if the SVD of Q_{SOM} results in null singular values, the system is unobservable.

5. Degree of Observability

The rank of Q_{SOM} only informs whether the system is observable or not. The observability condition of the states, in particular, cannot be evaluated by the rank analysis. For LTI systems, the observability of the states can be obtained directly from analytical expressions, using similarity transformations that decompose the system into observable and unobservable subspaces [8,21]. However, the observation model and the dynamic model of the navigation errors, presented in Section 2, are LTV. So, it is hard to obtain analytical expressions for the observability of the states.

Alternatively, the concept degree of observability can be used. The degree of observability informs how observable the state of the system is.

Usual methods to evaluate the observability degree of a state rely on the Q_{SOM} singular value decomposition approach [11,13,15,26]. In particular, the degree of observability can be determined using the weighted singular vector u_r [11,26]:

$$u_r = \sum_{i=1}^{r} \frac{\sigma_i}{\sigma_1} u_i \tag{33}$$

Equation (33) represents the weighted singular vector for the first r singular vectors of U. The elements of a greater magnitude of u_r correspond to the states with a higher degree of observability, which, hence, can be determined as follows:

$$n_j = \frac{u_r(j)}{u_{r0}} \tag{34}$$

where u_{r0} corresponds to the elements of u_r associated with the measured states.

Note that the correspondence of the elements of u_r with the degree of observability is direct and independent of the measurements. In practical terms, the weighted singular vector allows for computing the degree of observability using only the observability matrix of the system.

6. Results

This section presents simulation results aiming at the observability analysis of the initial alignment and calibration of the AUV navigation sensors, subject to the following maneuver conditions:

1. Stationary.
2. Mooring. For a mooring maneuver, the vehicle motion was modeled with oscillations in roll (ϕ), pitch (θ), and yaw (ψ), with the same amplitude and period, and with oscillatory translational movement in the surge (x), sway (y), and heave (z) axes, also

with the same amplitude and period. For roll, pitch, and yaw, the model is given by the following (in deg):

$$\phi, \theta, \psi = 0° + 5.0° \sin\left(\frac{2\pi t}{10}\right)$$

For the translational movements (in m/s):

$$v_x, v_y, v_z = 0 + 0.1 \sin\left(\frac{2\pi t}{10}\right)$$

3. Straight-line with constant speed. In the straight-line maneuver with a constant speed, the velocity was set to 1.0 m/s in the x-axis, and 0 in the y and z axes. The swing movement was disregarded.
4. Straight-line with acceleration. In this maneuver, the velocities in the y and z axes, as well as the oscillations in roll, pitch, and yaw, were null. The velocity model in the x-axis is given by the following (in m/s):

$$v_x = 1.5 + 0.75 \sin\left(\frac{2\pi t}{10}\right)$$

Therefore, the resulting acceleration in the x-axis (in m/s^2) is as follows: $a_x = \frac{1.5\pi}{10} \cos\left(\frac{2\pi t}{10}\right)$.

5. Zigzag. In the zigzag maneuver, the speed was set to 1.0 m/s in the x-axis, and 0 in the y and z axes. The roll and pitch oscillations were 0. The yaw oscillation model is given by the following (in deg): $\psi = 0° + 5.0° \sin\left(\frac{2\pi t}{10}\right)$.
6. Lawn mower with constant speed. In the lawn mower maneuver, the velocity was set to 1.0 m/s in the x-axis, and zero in the y and z axes. The swing movement was disregarded.
7. Lawn mower with zigzag and swing. For this maneuver, roll and pitch oscillations were null. For yaw, the oscillation model is given by the following (in deg):

$$\psi = 0° + 5.0° \sin\left(\frac{2\pi t}{10}\right)$$

The velocity models (in m/s) are given by the following:

$$v_x = 1.0 + 0.05 \sin\left(\frac{2\pi t}{10}\right)$$

$$v_y = v_z = 0.1 \sin\left(\frac{2\pi t}{10}\right)$$

All maneuvers lasted 1 h. For the stationary maneuver, analytical expressions were obtained for the observability of the states, as, for this condition, the dynamic and observation models are LIT. Regarding the degrees of observability of the state variables, they were calculated using Equation (34). The following assumptions were additionally considered:

1. AUV aligned with the navigation frame (NED).
2. Initial coordinates of -23 degrees (latitude) and -45 degrees (longitude).
3. Zero initial altitude.
4. IMU/DVL misalignment and DVL scale factor error are null.
5. Loosely coupled INS/GPS/DVL/PS, INS/DVL/PS, and INS/DVL integrations, with dynamic and observational models, as given by Equations (1), (15), (17), and (19).

6.1. Observability Decomposition: Stationary Case

For the INS/GPS/DVL/PS integration, the rank of Q_o is 12. So, the dimension of the unobservable subspace is equal to 7. Applying the similarity transformation given by

Equation (35), where W is a matrix of *r* vectors of the canonical base of $\Re^{19}$ and linearly independent of the kernel of Q_o.

$$\bar{x} = Tx = \left[\begin{array}{c} \bar{x}_o \\ \bar{x}_{\bar{o}} \end{array} \right] \tag{35}$$

$$T = \left[\begin{array}{cc} W & \ker(Q_o) \end{array} \right]^{-1} \tag{36}$$

$$\ker(Q_0) = \left[\begin{array}{ccccccc}
0 & 0 & \frac{1}{g} & 0 & 0 & 0 & 0 \\
0 & -\frac{1}{g} & 0 & 0 & 0 & 0 & 0 \\
\frac{1}{\Omega\cos(L)} & 0 & -\frac{\tan(L)}{g} & 0 & 0 & 0 & 0 \\
0 & 0 & 0 & 0 & 0 & 0 & 0 \\
0 & 0 & 0 & 0 & 0 & 0 & 0 \\
0 & 0 & 0 & 0 & 0 & 0 & 0 \\
0 & 0 & 0 & 0 & 0 & 0 & 0 \\
0 & 0 & 0 & 0 & 0 & 0 & 0 \\
0 & 0 & 0 & 0 & 0 & 0 & 0 \\
0 & \frac{\Omega\sin(L)}{g} & 0 & 0 & 0 & 0 & 0 \\
1 & 0 & 0 & 0 & 0 & 0 & 0 \\
0 & \frac{\Omega\cos(L)}{g} & 0 & 0 & 0 & 0 & 0 \\
0 & 1 & 0 & 0 & 0 & 0 & 0 \\
0 & 0 & 1 & 0 & 0 & 0 & 0 \\
0 & 0 & 0 & 0 & 0 & 0 & 0 \\
0 & 0 & 0 & 1 & 0 & 0 & 0 \\
0 & 0 & 0 & 0 & 1 & 0 & 0 \\
0 & 0 & 0 & 0 & 0 & 1 & 0 \\
0 & 0 & 0 & 0 & 0 & 0 & 1
\end{array} \right] \tag{37}$$

The following states and combinations of states are found to be observable:

$$\bar{x}_o = \left[\begin{array}{c}
\phi_N - \frac{b_{ay}}{g} \\
\phi_E + \frac{b_{ax}}{g} \\
\phi_D - \frac{b_{gy}}{\Omega\cos(L)} + \frac{\tan(L)b_{ay}}{g} \\
\delta v_N \\
\delta v_E \\
\delta v_D \\
\delta L \\
\delta\lambda \\
\delta h \\
b_{gx} - \frac{\Omega\sin(L)b_{ax}}{g} \\
b_{gz} - \frac{\Omega\cos(L)b_{ax}}{g} \\
b_{az}
\end{array} \right] \tag{38}$$

The unobservable states, in turn, are as follows:

$$\bar{x}_o = \left[\begin{array}{c}
b_{gy} \\
b_{ax} \\
b_{ay} \\
e_x \\
e_y \\
e_z \\
s_f
\end{array} \right] \tag{39}$$

As can be inferred, all of the states are individually unobservable for the stationary condition, except for the velocity errors, the position errors, and the accelerometer bias in the z-axis (b_{az}).

Considering the INS/DVL/PS integration, the rank of Q_o is equal to 10, hence the dimension of the unobservable subspace becomes 9. Applying the similarity transformation, the kernel of Q_o is:

$$
\ker(Q_0) = \begin{bmatrix}
0 & 0 & 0 & 0 & \frac{1}{g} & 0 & 0 & 0 & 0 \\
0 & 0 & 0 & -\frac{1}{g} & 0 & 0 & 0 & 0 & 0 \\
0 & \frac{1}{\Omega\cos(L)} & 0 & 0 & -\frac{\tan(L)}{g} & 0 & 0 & 0 & 0 \\
0 & 0 & 0 & 0 & 0 & 0 & 0 & 0 & 0 \\
0 & 0 & 0 & 0 & 0 & 0 & 0 & 0 & 0 \\
0 & 0 & 0 & 0 & 0 & 0 & 0 & 0 & 0 \\
0 & 0 & -\frac{1}{\Omega\cos(L)} & \frac{1}{g} & 0 & 0 & 0 & 0 & 0 \\
1 & 0 & 0 & 0 & 0 & 0 & 0 & 0 & 0 \\
0 & 0 & 0 & 0 & 0 & 0 & 0 & 0 & 0 \\
0 & 0 & \tan(L) & 0 & 0 & 0 & 0 & 0 & 0 \\
0 & 1 & 0 & 0 & 0 & 0 & 0 & 0 & 0 \\
0 & 0 & 1 & 0 & 0 & 0 & 0 & 0 & 0 \\
0 & 0 & 0 & 1 & 0 & 0 & 0 & 0 & 0 \\
0 & 0 & 0 & 0 & 1 & 0 & 0 & 0 & 0 \\
0 & 0 & 0 & 0 & 0 & 0 & 0 & 0 & 0 \\
0 & 0 & 0 & 0 & 0 & 1 & 0 & 0 & 0 \\
0 & 0 & 0 & 0 & 0 & 0 & 1 & 0 & 0 \\
0 & 0 & 0 & 0 & 0 & 0 & 0 & 1 & 0 \\
0 & 0 & 0 & 0 & 0 & 0 & 0 & 0 & 1
\end{bmatrix} \tag{40}
$$

The observable states and combinations of states are, then:

$$
\bar{x}_o = \begin{bmatrix}
\phi_N - \frac{b_{ay}}{g} \\
\phi_E - \frac{b_{ax}}{g} \\
\phi_D - \frac{b_{gy}}{\Omega\cos(L)} + \frac{\tan(L)b_{ay}}{g} \\
\delta v_N \\
\delta v_E \\
\delta v_D \\
\delta h \\
b_{gx} + \Omega\sin(L)\delta L - \frac{\Omega\sin(L)b_{ax}}{g} \\
b_{gx} + \Omega\cos(L)\delta L - \frac{\Omega\cos(L)b_{ax}}{g} \\
b_{az}
\end{bmatrix} \tag{41}
$$

The unobservable states and combinations of states, in turn, are as follows:

$$
\bar{x}_o = \begin{bmatrix}
\delta\lambda \\
b_{gy} \\
\frac{\Omega\cos(L)b_{ax}}{g} - \Omega\cos(L)\delta L \\
b_{ax} \\
b_{ay} \\
e_x \\
e_y \\
e_z \\
s_f
\end{bmatrix} \tag{42}
$$

For the INS/DVL/PS integration, hence, all of the states are individually unobservable, except the velocity errors, the altitude error (δh), and the accelerometer bias in the z-axis. Furthermore, the gyro biases in the x (b_{gx}) and z (b_{gz}) axes are coupled with the latitude error (δL), unlike the result of the INS/GPS/DVL/PS integration shown in Equation (38). In such an integration, b_{gx} and b_{gz} are coupled only with the accelerometer bias in the x-axis (b_{ax}).

For the INS/DVL integration, it is possible to show that the rank of Q_o is equal to 9, which makes the dimension of the unobservable subspace equal to 10. The kernel of Q_o, in this case, is as follows:

$$
\ker(Q_0) =
\begin{bmatrix}
0 & 0 & 0 & 0 & \frac{1}{g} & 0 & 0 & 0 & 0 & 0 \\
0 & 0 & 0 & -\frac{1}{g} & 0 & 0 & 0 & 0 & 0 & 0 \\
0 & \frac{1}{\Omega\cos(L)} & 0 & 0 & -\frac{\tan(L)}{g} & 0 & 0 & 0 & 0 & 0 \\
0 & 0 & 0 & 0 & 0 & 0 & 0 & 0 & 0 & 0 \\
0 & 0 & 0 & 0 & 0 & 0 & 0 & 0 & 0 & 0 \\
0 & 0 & 0 & 0 & 0 & 0 & 0 & 0 & 0 & 0 \\
0 & 0 & -\frac{1}{\Omega\cos(L)} & \frac{1}{g} & 0 & 0 & 0 & 0 & 0 & 0 \\
1 & 0 & 0 & 0 & 0 & 0 & 0 & 0 & 0 & 0 \\
0 & 0 & 0 & 0 & 0 & \frac{R_0+h}{2g} & 0 & 0 & 0 & 0 \\
0 & 0 & \tan(L) & 0 & 0 & 0 & 0 & 0 & 0 & 0 \\
0 & 1 & 0 & 0 & 0 & 0 & 0 & 0 & 0 & 0 \\
0 & 0 & 1 & 0 & 0 & 0 & 0 & 0 & 0 & 0 \\
0 & 0 & 0 & 1 & 0 & 0 & 0 & 0 & 0 & 0 \\
0 & 0 & 0 & 0 & 1 & 0 & 0 & 0 & 0 & 0 \\
0 & 0 & 0 & 0 & 0 & 1 & 0 & 0 & 0 & 0 \\
0 & 0 & 0 & 0 & 0 & 0 & 1 & 0 & 0 & 0 \\
0 & 0 & 0 & 0 & 0 & 0 & 0 & 1 & 0 & 0 \\
0 & 0 & 0 & 0 & 0 & 0 & 0 & 0 & 1 & 0 \\
0 & 0 & 0 & 0 & 0 & 0 & 0 & 0 & 0 & 1 \\
\end{bmatrix}
\tag{43}
$$

The observable states and combinations of states are as follows:

$$
\overline{x}_o =
\begin{bmatrix}
\phi_N - \frac{b_{ay}}{g} \\
\phi_E + \frac{b_{ax}}{g} \\
\phi_D - \frac{b_{gy}}{\Omega\cos(L)} + \frac{\tan(L)b_{ay}}{g} \\
\delta v_N \\
\delta v_E \\
\delta v_D \\
b_{gx} + \Omega \sin(L)\delta L - \frac{\Omega\sin(L)b_{ax}}{g} \\
b_{gz} + \Omega\cos(L)\delta L - \frac{\Omega\cos(L)b_{ax}}{g} \\
b_{az} - \frac{2g\delta h}{R_0+h}
\end{bmatrix}
\tag{44}
$$

While the unobservable states and combinations of states are as follows:

$$\overline{x}_o = \begin{bmatrix} \delta\lambda \\ b_{gy} \\ \frac{\Omega\cos(L)b_{ax}}{g} - \Omega\cos(L)\delta L \\ b_{ax} \\ b_{ay} \\ \frac{2g\delta h}{R_0+h} \\ e_x \\ e_y \\ e_z \\ s_f \end{bmatrix} \qquad (45)$$

For the INS/DVL integration, it can be seen that all states are individually unobservable, except for the velocity errors. The gyro biases b_{gx} and b_{gz} are coupled with the latitude error and the accelerometer bias in the x-axis. In addition, b_{az} is coupled with the altitude error, δh, which does not occur in the INS/GPS/DVL/PS and INS/DVL/PS integrations.

The analytical expressions for the observability of the states, obtained for the stationary case, show that the addition of position errors (latitude, longitude, and altitude) in the observation vector not only increases the dimension of the observable subspace, but also decouples b_{gx} and b_{gz} from δL, and b_{az} from δh. In practical terms, decoupling b_{gx}, b_{gz}, and b_{az} from latitude and altitude errors improves the accuracy of estimation of these variables.

6.2. Comparison Results for INS/GPS/DVL/PS Integration

Table 1 shows the results of the system observability analysis performed by the rank computation of Q_{SOM}. For the stationary maneuver, the rank of Q_{SOM} is 12. This value is in accordance with the rank of Q_o obtained in Section 6.1. In addition, it can be seen that the system is observable only for the lawn mower with zigzag and swing maneuver.

Table 1. Observability and final rank of Q_{SOM} ($j = 100$). INS/GPS/DVL/PS integration.

Maneuver	Q_{SOM} Rank	System Observability
Stationary	12	Unobservable
At Mooring	18	Unobservable
Straight-line	18	Unobservable
Straight-line with acceleration	18	Unobservable
Zigzag	18	Unobservable
Lawn Mower	18	Unobservable
Lawn Mower with zigzag and swing	19	Observable

The comparative results of the degree of observability for the state variables are illustrated in Figures 1–4. Figure 1 shows that the degree of observability of ϕ_D was higher for the straight-line with the acceleration maneuver (yellow bar), lawn mower maneuvers (green and dark blue bars), and zigzag (middle blue bar). Likewise, ϕ_N and ϕ_E obtained a higher degree of observability for lawn mower, straight-line with acceleration, and zigzag.

The lowest degrees of observability of ϕ_N and ϕ_E were obtained for stationary (light blue bar) and straight-line with constant speed (gray bar) maneuvers. For ϕ_D, the lowest degrees of observability were obtained for stationary, straight-line with constant speed, and mooring maneuvers (orange bar).
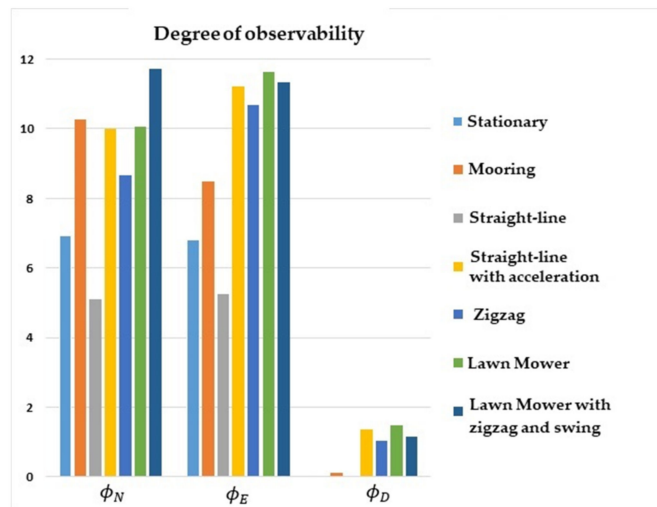
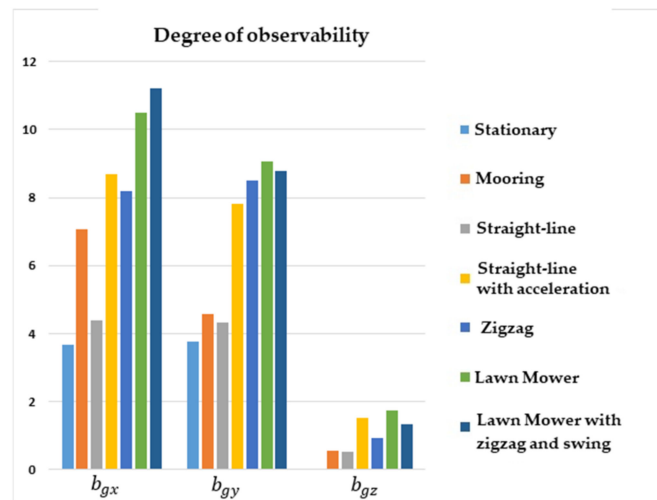**Figure 1.** Degrees of observability of the attitude errors. INS/GPS/DVL/PS integration.

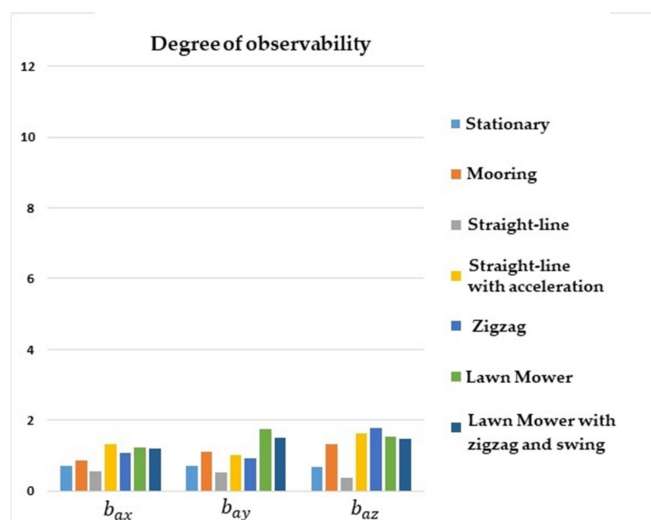**Figure 2.** Degrees of observability of the gyro biases. INS/GPS/DVL/PS integration.

Figure 3. Degrees of observability of the accelerometer biases. INS/GPS/DVL/PS integration.
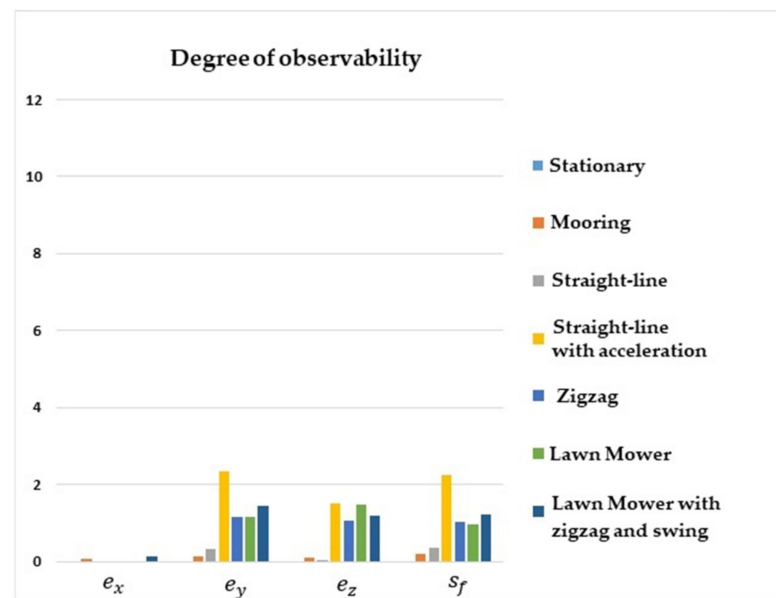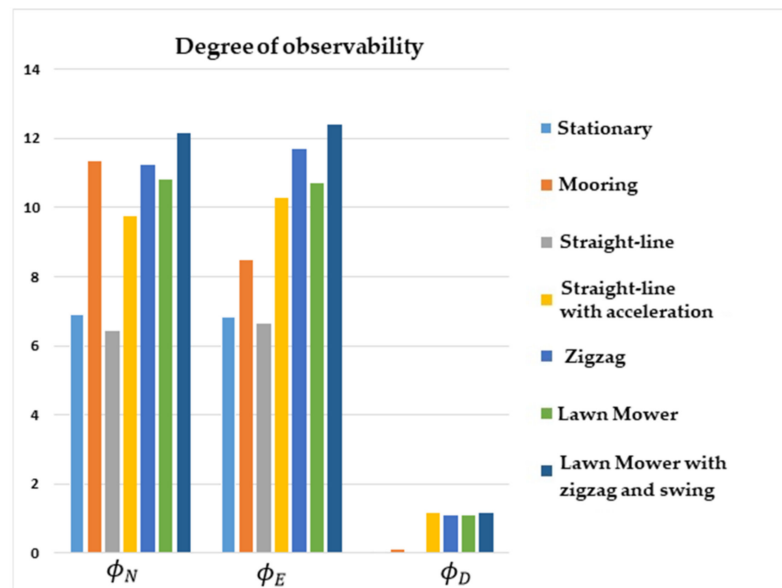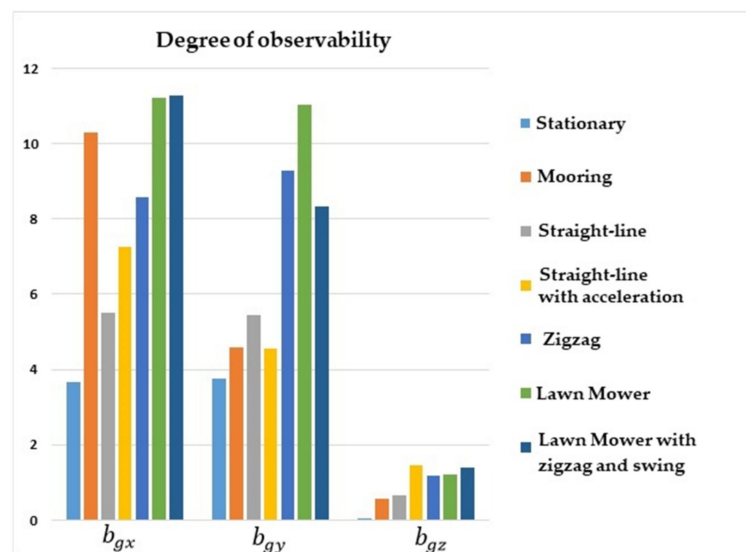
Figure 4. Degrees of observability of the IMU/DVL misalignment and the DVL scale factor error. INS/GPS/DVL/PS integration.

Figure 2 shows that the degrees of observability for b_{gx} and b_{gy} were lower for the stationary and straight-line with constant speed maneuvers, and higher for lawn mower, straight-line with acceleration, and zigzag. Concerning b_{gz}, the degree of observability was lower for stationary, mooring, and straight-line with constant speed maneuvers, and was higher for lawn mower and straight-line with acceleration.

Figure 3 shows that the degrees of observability of b_{ax}, b_{ay}, and b_{az} were higher for lawn mower maneuvers, straight-line with acceleration, zigzag, and mooring. For the stationary maneuver and straight-line with a constant speed, the degrees of observability of the accelerometer biases were lower. In general, it can be seen that maneuvers in which there were no changes of direction or oscillation resulted in lower degrees of observability for the accelerometer biases.

Figure 4 shows that the degrees of observability of e_y, e_z, and s_f were higher for the straight-line with acceleration maneuver, lawn mower, and zigzag. For the stationary, straight-line with constant speed, and mooring maneuvers, the degrees of observability of e_y, e_z, and s_f were lower. Regarding e_x, the degree of observability was higher for the mooring and lawn mower with zigzag and swing maneuvers.

It is interesting to note that the degree of observability of e_x was improved for the mooring and lawn mower with zigzag and swing maneuvers, as these scenarios induced velocity components in the y and z axes of the vehicle.

6.3. Comparison Results for INS/DVL/PS Integration

Unlike the INS/GPS/DVL/PS integration, Table 2 shows that the INS/DVL/PS integration made the system unobservable for all of the maneuvers evaluated. This result was already expected, as the longitude and latitude errors were unobservable states for INS/DVL/PS integration. Furthermore, for the stationary maneuver, the rank of $\mathbf{Q_{SOM}}$ was found to be 10, whose value was in agreement with the rank of Q_o obtained in Section 6.1.

The comparative results of the degree of observability for the INS/DVL/PS integration are illustrated in Figures 5–8. Figure 5, in particular, shows that the degrees of observability of the attitude errors were higher for lawn mower, zigzag, and straight-line with acceleration maneuvers. The degrees of observability of ϕ_N and ϕ_E were lower for stationary and straight-line with constant speed maneuvers. Concerning ϕ_D, the degree of observability was smaller for stationary maneuver, straight-line with constant speed, and mooring.

Table 2. Observability and final rank of Q_{SOM} ($j = 100$). INS/DVL/PS integration.

Maneuver	Q_{SOM} Rank	System Observability
Stationary	10	Unobservable
At Mooring	17	Unobservable
Straight-line	16	Unobservable
Straight-line with acceleration	17	Unobservable
Zigzag	17	Unobservable
Lawn Mower	17	Unobservable
Lawn Mower with zigzag and swing	18	Unobservable

Figure 5. Degrees of observability of the attitude errors. INS/DVL/PS integration.

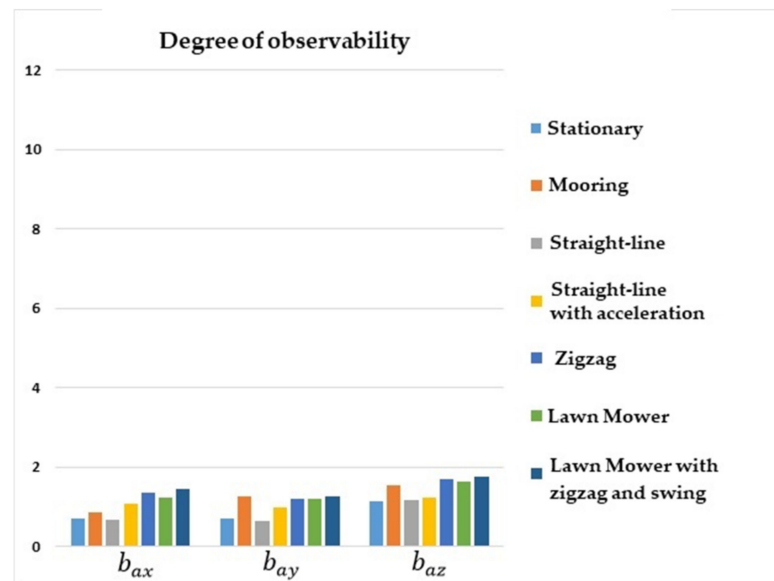**Figure 6.** Degrees of observability of the gyro biases. INS/DVL/PS integration.

Figure 7. Degrees of observability of the accelerometer biases. INS/DVL/PS integration.
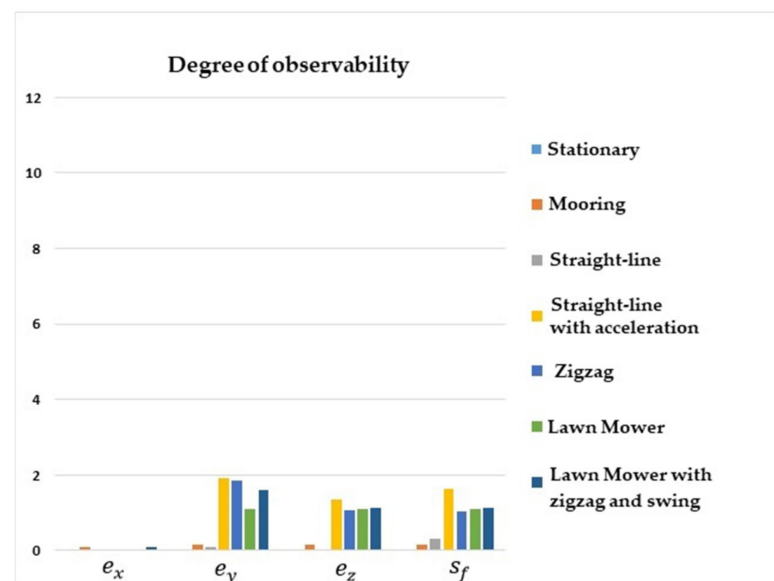

Figure 8. Degrees of observability of the IMU/DVL misalignment and the DVL scale factor error. INS/DVL/PS integration.

Figure 6 shows that the lowest degrees of observability for b_{gx} were obtained for the stationary and straight-line with constant speed maneuvers, and the highest degrees for mooring, lawn mower, and zigzag maneuvers. Regarding b_{gy}, the lowest degrees of observability were obtained for the stationary, mooring, and straight-line maneuvers, and the highest degrees were for lawn mower and zigzag. For b_{gz}, the lowest degrees of observability were obtained for the stationary, mooring, and straight-line with constant speed maneuvers, and the highest were for lawn mower, zigzag, and straight-line with acceleration maneuvers.

Concerning the accelerometer biases, Figure 7 shows that the degree of observability of b_{ax} was higher for lawn mower maneuvers, straight line with acceleration, and zigzag, and lower for stationary, mooring, and straight line with constant speed maneuvers. For b_{ay} and b_{az}, the degree of observability was higher for maneuvers with acceleration or oscillation. It is worthy of note that, although the degrees of observability of the accelerometer biases

were increased with lawn mower and zigzag maneuvers, the differences with respect to the remaining maneuvers were not significant.

Lastly, and as also observed for INS/GPS/DVL/PS integration, Figure 8 shows that the degrees of observability of e_y, e_z, and s_f were higher for the lawn mower, zigzag, and straight-line with acceleration maneuvers. The degrees of observability were lower, in turn, for the stationary, straight-line with constant speed, and mooring scenarios. Regarding e_x, the degree of observability was higher for the mooring and lawn mower with zigzag and swing maneuvers.

6.4. Comparison Results for INS/DVL Integration

Table 3 shows that the system was unobservable for all of the maneuvers evaluated using the simplified INS/DVL integration scheme. This result was again already expected as the position errors were unobservable states for the INS/DVL integration. In addition, for stationary maneuver, the rank of Q_{SOM} was 9, whose value was equal to the rank of Q_o obtained in Section 6.1.

Table 3. Observability and final rank of Q_{SOM} ($j = 100$). INS/DVL integration.

Maneuver	Q_{SOM} Rank	System Observability
Stationary	9	Unobservable
At Mooring	17	Unobservable
Straight-line	15	Unobservable
Straight-line with acceleration	16	Unobservable
Zigzag	16	Unobservable
Lawn Mower	16	Unobservable
Lawn Mower with zigzag and swing	17	Unobservable

Figures 9–12 show the comparative results of the degree of observability for the INS/DVL integration. As illustrated in Figure 9, the highest degrees of observability for ϕ_N and ϕ_E were obtained for the zigzag maneuver. The lowest degrees of observability for ϕ_N and ϕ_E, in turn, were obtained for the stationary maneuver. Regarding ϕ_D, the highest degrees of observability were obtained for the lawn mower and zigzag maneuvers. On the contrary, the lowest degrees were obtained for the stationary, mooring, and straight-line with constant speed scenarios.
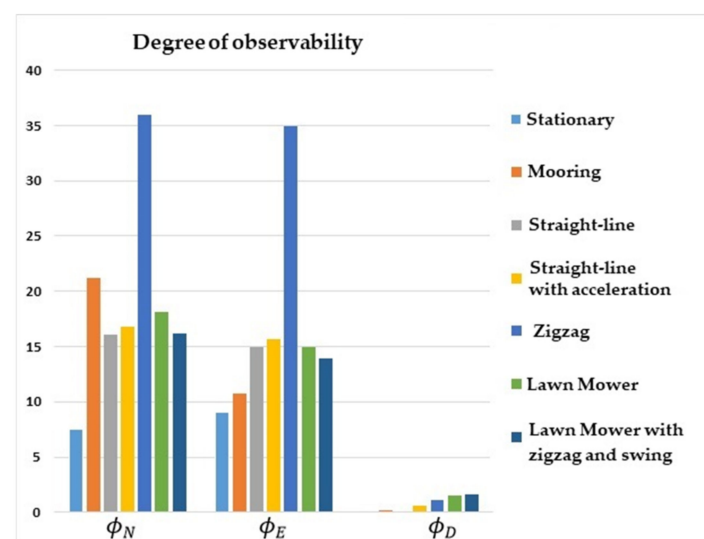

Figure 9. Degrees of observability of the attitude errors. INS/DVL integration.
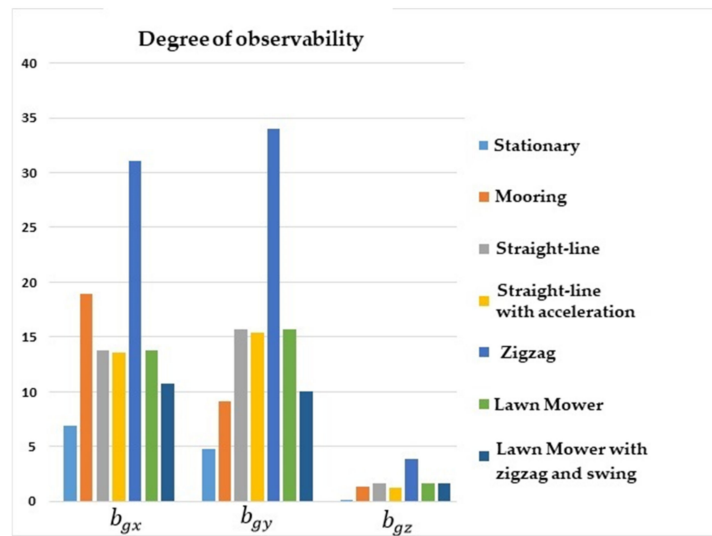
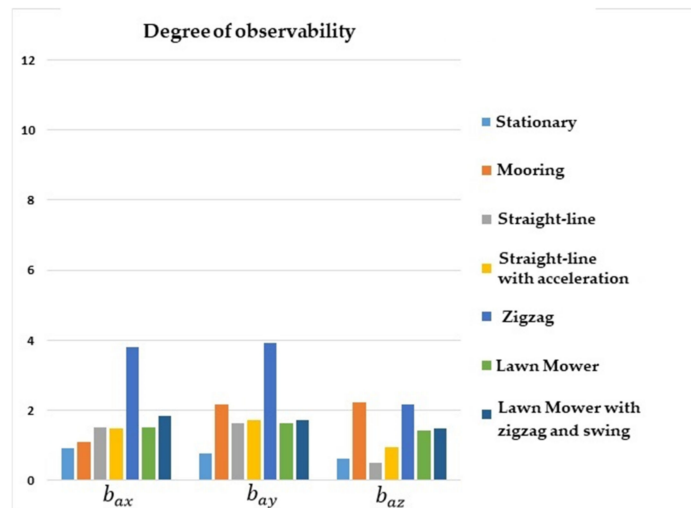**Figure 10.** Degrees of observability of the gyro biases. INS/DVL integration.

Figure 11. Degrees of observability of the accelerometer biases. INS/DVL integration.
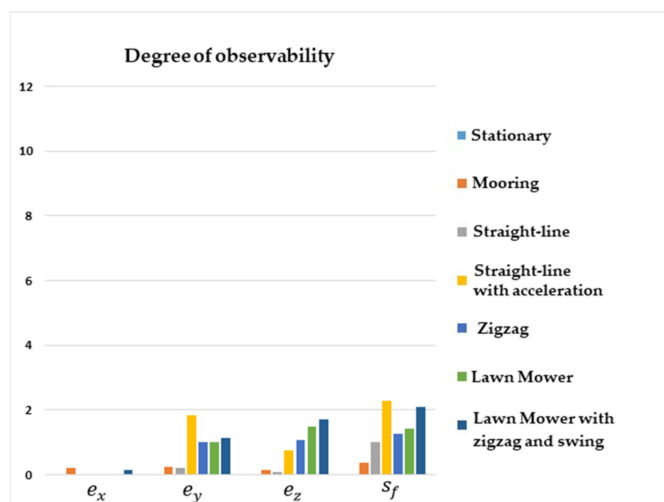

Figure 12. Degrees of observability of the IMU/DVL misalignment and the DVL scale factor error. INS/DVL integration.

Concerning the gyro biases, the degrees of observability were lower for the stationary maneuver, and higher for zigzag, as illustrated in Figure 10. For the accelerometer biases, Figure 11 shows that the degrees of observability were higher for zigzag and mooring (b_{az}), and lower for the stationary maneuver.

Concerning e_y, e_z, and s_f, Figure 12 shows that the degrees of observability were higher for the maneuvers of lawn mower, zigzag, and straight-line with acceleration. The degrees of observability were lower, however, for the stationary maneuver, straight-line with constant speed, and mooring. Regarding e_x, finally, its degree of observability was found to be higher for the mooring and lawn mower with zigzag and swing maneuvers.

7. Discussion

The observability decomposition performed for the stationary case showed that the addition of the position errors in the observation vector decoupled the biases b_{gx}, b_{gz}, and b_{az} from the latitude (b_{gx} and b_{gz}) and altitude errors (b_{az}). Furthermore, maneuvers including changes of direction and speed excitation in the three axes increased the dimension of the observable subspace. For the INS/GPS/DVL/PS integration, in particular, the system became fully observable for these types of maneuvers.

In addition, the simulation results showed that the alignment errors obtained higher degrees of observability for the lawn mower, zigzag (especially for INS/DVL), and straight-line with acceleration maneuvers, while the lower degrees of observability for the stationary and straight-line at constant speed maneuvers. In particular, ϕ_D was shown to possess the lowest degree of observability among the attitude errors.

For the three integration schemes evaluated, the degree of observability of ϕ_D was increased by accelerating the AUV in the local navigation frame, especially in the horizontal plane (which corresponds to the straight-line with acceleration, zigzag, and lawn mower maneuvers). For the lawn mower with zigzag and swing maneuver, the change of orientation in the horizontal plane additionally provoked velocity variations in the NED frame, which produced acceleration components in the north and east directions. The influence of such accelerations on the degree of observability of ϕ_D has also been observed by other authors [12,14,15,27].

Regarding the gyro biases, the simulation results showed that the degree of observability of b_{gz} was increased with vertical oscillation or acceleration in the x-axis. Particularly for INS/DVL integration, the degree of observability of b_{gz} was higher for the zigzag maneuver. Furthermore, the zigzag and lawn mower maneuvers also improved the degrees of observability of the accelerometer biases. As demonstrated in [18], the estimations of the accelerometer biases were improved with angular movements.

Finally, the degrees of observability of the IMU/DVL misalignment in the y and z axes, as well as, the DVL scale factor error, were significantly increased by the occurrence of translational motion. Specifically, for e_x, the degree of observability was improved with translational movements in the y and z axes of the AUV. This condition was also evidenced in [19] for a simplified model, in which the orientation and the velocity of the vehicle were perfectly known. In [18], it was demonstrated that the AUV displacement in the z-axis with constant attitude enabled the estimation of e_x in single-thruster AUVs. It is noteworthy that e_x, e_y, e_z and s_f were individually unobservable for the stationary case, regardless of the three integrations schemes evaluated, which means that the calibration of the DVL with stationary AUV is not possible to be performed.

Despite being relevant, the degree of observability analysis did not allow us to visualize the couplings between the state variables. This has only been possible for the stationary case, via observability decomposition, which evidenced the existence of the couplings $\{\phi_N, b_{ay}\}$ and $\{\phi_E, b_{ax}\}$, as well as the couplings between ϕ_D, b_{gy}, and b_{ay}. These results are in agreement with the traditional literature [21–23,28].

Additionally, the observability decomposition for the stationary case showed that b_{ax}, b_{ay}, and b_{gy} are variable states of the unobservable subspace. Regarding b_{gx} and b_{gz}, they can be considered individually observable, as their couplings with b_{ax}, that is,

$\left\{ b_{gx}, -\frac{\Omega \sin(L) b_{ax}}{g} \right\}$ and $\left\{ b_{gz}, -\frac{\Omega \cos(L) b_{ax}}{g} \right\}$, are negligible, given that the magnitudes of the weighting coefficients of b_{ax} are less than 10^{-5} rad.s/m.

It is also noteworthy that the degree of observability obtained for b_{gy} was close to b_{gx} and significantly higher than b_{gz}. Such results are in agreement with previous works [12,14,15], but raises the question that the degree of observability may not be directly related to the estimation accuracy of the states, given that b_{gx} and b_{gz} are recognizably known to be better estimated than b_{gy} in the AUV initial alignment and calibration problem [23].

Therefore, the simulation results presented in this paper suggest that the exclusive analysis of the degree of observability may not be a suitable metrics for the "estimability" of the states. As defined by Baram and Kailath [29], the estimability of a system is the ability to reduce the mean squared error in the estimation of the states. As suggested by the authors, the estimability analysis can be seen as a complementary tool to the observability analysis. In [9], for instance, observability and estimability analyses were carried out separately for the space situational awareness (SSA) problem. The observability analysis, in terms of the observability matrix rank, aimed to inform whether the measurements were sufficient for the estimation of the states. Conversely, the estimability analysis aimed to evaluate the performance of the estimation.

8. Conclusions

In this work, the effects of different maneuvers and integration schemes on the AUV initial alignment and calibration were analyzed in terms of system's observability and state variables' degree of observability. The simulation results showed that the system became fully observable for INS/GPS/DVL/PS integration when lawn mower with zigzag and swing maneuvers were carried out.

For the three investigated integrations, the observability degrees of the IMU/DVL misalignment and the DVL scale factor error were increased with translational motion. In addition, the degrees of observability of the inertial sensor biases and the vertical alignment error were increased with maneuvers encompassing changes of direction. The observability degrees of the vertical alignment error and the gyro bias in the z-axis, lastly, were increased by accelerating the AUV along its longitudinal axis.

Finally, the simulation results presented in this article suggest that the exclusive analysis of the degree of observability may not be an adequate metric for the "estimability" of the states. In this sense, a thorough investigation on the physical meaning of the degree of observability and its relation with the estimability of states, specifically in the scope of the AUV initial alignment and calibration problem, will be a topic for future investigation by the authors.

Author Contributions: Conceptualization, A.F., F.O.S., E.A.d.B.; methodology, A.F.; software, A.F.; validation, A.F.; formal analysis, A.F., F.O.S.; investigation, A.F., F.O.S., E.A.d.B.; resources, A.F., E.A.d.B.; data curation, A.F.; writing—A.F., F.O.S. and E.A.d.B.; visualization, A.F.; supervision, F.O.S. and E.A.d.B.; project administration E.A.d.B.; funding acquisition, E.A.d.B. All authors have read and agreed to the published version of the manuscript.

Informed Consent Statement: Not applicable.

References

1. Almalki, F.A.; Alsamhi, S.H.; Sahal, R.; Hassan, J.; Hawbani, A.; Rajput, N.S.; Saif, A.; Morgan, J.; Breslin, J. Green IoT for Eco-Friendly and Sustainable Smart Cities: Future Directions and Opportunities. *Mob. Netw. Appl.* **2021**, 1–25. [CrossRef]
2. Alsamhi, S.H.; Afghah, F.; Sahal, R.; Hawbani, A.; Al-Qaness, M.A.A.; Lee, B.; Guizani, M. Green internet of things using UAVs in B5G networks: A review of applications and strategies. *Ad Hoc Netw.* **2021**, *117*, 102505. [CrossRef]
3. Bagnitsky, A.; Inzartsev, A.; Pavin, A.; Melman, S.; Morozov, M. Side Scan Sonar using for Underwater Cables & Pipelines Tracking by Means of AUV. In Proceedings of the 2011 IEEE Symposium on Underwater Technology and Workshop on Scientific Use of Submarine Cables and Related Technologies, Tokyo, Japan, 5–8 April 2011.
4. Alsamhi, S.H.; Ma, O.; Ansari, M.S. Convergence of Machine Learning and Robotics Communication in Collaborative Assembly: Mobility, Connectivity and Future Perspectives. *J. Intell. Robot. Syst.* **2019**, *98*, 541–566. [CrossRef]
5. Jo, K.; Kim, J.; Kim, D.; Jang, C.; Sunwoo, M. Development of Autonomous Car—Part II: A Case Study on the Implementation of an Autonomous Driving System Based on Distributed Architecture. *IEEE Trans. Ind. Electron.* **2015**, *62*, 5119–5132. [CrossRef]
6. Paull, L.; Saeedi, S.; Seto, M.; Li, H. AUV Navigation and Localization: A Review. *IEEE J. Ocean. Eng.* **2014**, *39*, 131–149. [CrossRef]
7. Goshen-Meskin, D.; Bar-Itzhack, I. Observability analysis of piece-wise constant systems. I. Theory. *IEEE Trans. Aerosp. Electron. Syst.* **1992**, *28*, 1056–1067. [CrossRef]
8. Chen, C.-T. *Linear System Theory and Design*, 3rd ed.; Oxford University Press: New York, NY, USA, 1999.
9. Friedman, A.M. Observability Analysis for Space Situational Awareness. Ph.D. Thesis, Purdue University, West Lafayette, IN, USA, 2020.
10. Kalman, R.E. A New Approach to Linear Filtering and Prediction Problems. *J. Basic Eng.* **1960**, *82*, 35–45. [CrossRef]
11. Doren, J.F.M.V. Model Structure Analysis for Model-based Operation of Petroleum Reservoirs. Ph.D. Thesis, Technical University, Delft, The Netherlands, 2010.
12. Wu, Z.; Yao, M.; Ma, H.; Jia, W. Improving Accuracy of the Vehicle Attitude Estimation for Low-Cost INS/GPS Integration Aided by the GPS-Measured Course Angle. *IEEE Trans. Intell. Transp. Syst.* **2013**, *14*, 553–564. [CrossRef]
13. Jinyan, M.; Quanbo, G.; Teng, S. Impact analysis between observable degrees and estimation accuracy of Kalman filtering. In Proceedings of the2015 International Conference on Estimation, Detection and Information Fusion (ICEDIF), Harbin, China, 10–11 January 2015.
14. Wang, Q.; Yang, C.-S.; Wang, Y.-X. Study on the observability degree of integrated inertial navigation system of autonomous underwater vehicle. *Int. J. Embed. Syst.* **2020**, *12*, 359–370. [CrossRef]
15. Chen, W.; Yang, Z.; Gu, S.; Wang, Y.; Tang, Y. Adaptive transfer alignment method based on the observability analysis for airborne pod strapdown inertial navigation system. *Sci. Rep.* **2022**, *12*, 946. [CrossRef] [PubMed]
16. Zhang, Y. An approach of DVL-aided SDINS alignment for in-motion vessel. *Optik* **2013**, *124*, 6270–6275. [CrossRef]
17. Klein, I.; Diamant, R. Observability Analysis of DVL/PS Aided INS for a Maneuvering AUV. *Sensors* **2015**, *15*, 26818–26837. [CrossRef] [PubMed]
18. Pan, X.; Wu, Y. Underwater Doppler Navigation with Self-calibration. *J. Navig.* **2016**, *69*, 295–312. [CrossRef]
19. Liu, P.; Zhao, S.; Qing, L.; Ma, Y.; Lu, B.; Hou, D. A Calibration Method for DVL Measurement Errors Based on Observability Analysis. In Proceedings of the 2019 Chinese Control Conference (CCC), Guangzhou, China, 27–30 July 2019.
20. Liu, P.; Wang, B.; Hou, D.; Wang, K.; Zhu, Z. An Approach for DVL-Aided SINS In-Motion Alignment Based on Observability Analysis. *IEEE Sens. J.* **2021**, *21*, 17131–17143. [CrossRef]
21. Bar-Itzhack, I.Y.; Berman, N. Control theoretic approach to inertial navigation systems. *J. Guid. Control Dyn.* **1988**, *11*, 237–245. [CrossRef]
22. Silva, F.O.; Hemerly, E.M.; Leite Filho, W.C. On the Error State Selection for Stationary SINS Alignment and Calibration Kalman Filters—Part II: Observability/Estimability Analysis. *Sensors* **2017**, *17*, 439. [CrossRef] [PubMed]
23. Silva, F.O.; Hemerly, E.M.; Leite Filho, W.C. On the error state selection for stationary SINS alignment and calibration Kalman filters—Part I: Estimation algorithms. *Aerosp. Sci. Technol.* **2017**, *61*, 45–56. [CrossRef]
24. Shin, E.-H. Accuracy Improvement of Low Cost INS/GPS for Land Applications. Master's Thesis, University of Calgary, Calgary, AB, Canada, 2001.
25. Silva, F.O. Stationary Self-Alignment and Calibration Techniques for Strapdown Inertial Navigation Systems. Ph.D Thesis, Technological Institute of Aeronautics, Sao Jose dos Campos, Brazil, 2016.
26. Ruijter, R.B. Controllability and Observability of a 2D Wind Farm Model. Master's Thesis, Technical University, Delft, The Netherlands, 2017.
27. Salycheva, A.O.; Cannon, M. Kinematic Azimuth Alignment of INS using GPS Velocity Information. In Proceedings of the NTM 2004 Conference, San Diego, CA, USA, 26–28 January 2004.
28. Goshen-Meskin, D.; Bar-Itzhack, I. Observability analysis of piece-wise constant systems. II. Application to inertial navigation in-flight alignment. *IEEE Trans. Aerosp. Electron. Syst.* **1992**, *28*, 1068–1075. [CrossRef]
29. Baram, Y.; Kailath, T. Estimability and regulability of linear systems. In Proceedings of the 26th IEEE Conference on Decision and Control, Los Angeles, CA, USA, 9–11 December 1987; 1988; pp. 1116–1121.